Exact maps in density functional theory for lattice models

2016 New J. Phys. 18 083004

(http://iopscience.iop.org/1367-2630/18/8/083004)

New Journal of Physics
The open access journal at the forefront of physics

Deutsche Physikalische Gesellschaft DPG
IOP Institute of Physics

Published in partnership with: Deutsche Physikalische Gesellschaft and the Institute of Physics

OPEN ACCESS

RECEIVED
23 March 2016

REVISED
24 June 2016

ACCEPTED FOR PUBLICATION
8 July 2016

PUBLISHED
28 July 2016

PAPER

Exact maps in density functional theory for lattice models

Tanja Dimitrov[1,2,4], **Heiko Appel**[1,2], **Johanna I Fuks**[3] **and Angel Rubio**[1,2]

[1] Fritz-Haber-Institut der Max-Planck-Gesellschaft, Faradayweg 4-6, D-14195 Berlin-Dahlem, Germany
[2] Max-Planck-Institut für Struktur und Dynamik der Materie, Luruper Chaussee 149, D-22761 Hamburg, Germany
[3] Department of Physics and Astronomy, Hunter College and the Graduate Center of the City University of New York, 695 Park Avenue, New York, NY 10065, USA
[4] Author to whom any correspondence should be addressed.

E-mail: dimitrov@fhi-berlin.mpg.de, appel@fhi-berlin.mpg.de, johannafuks@gmail.com **and** angel.rubio@mpsd.mpg.de

Keywords: density functional theory, intrasystem steepening, derivative discontinuity, exact functional, density-to-potential map

Abstract

In the present work, we employ exact diagonalization for model systems on a real-space lattice to explicitly construct the exact density-to-potential and graphically illustrate the complete exact density-to-wavefunction map that underly the Hohenberg–Kohn theorem in density functional theory. Having the explicit wavefunction-to-density map at hand, we are able to construct arbitrary observables as functionals of the ground-state density. We analyze the density-to-potential map as the distance between the fragments of a system increases and the correlation in the system grows. We observe a feature that gradually develops in the density-to-potential map as well as in the density-to-wavefunction map. This feature is inherited by arbitrary expectation values as functional of the ground-state density. We explicitly show the excited-state energies, the excited-state densities, and the correlation entropy as functionals of the ground-state density. All of them show this exact feature that sharpens as the coupling of the fragments decreases and the correlation grows. We denominate this feature as *intra-system steepening* and discuss how it relates to the well-known inter-system derivative discontinuity. The inter-system derivative discontinuity is an exact concept for coupled subsystems with degenerate ground state. However, the coupling between subsystems as in charge transfer processes can lift the degeneracy. An important conclusion is that for such systems with a near-degenerate ground state, the corresponding cut along the particle number N of the exact density functionals is differentiable with a well-defined gradient near integer particle number.

1. Introduction

Over the last decades ground-state density-functional theory (DFT) has become a mature tool in material science and quantum chemistry [1–5]. Provided that the exact exchange-correlation (xc) functional is known, DFT is a formally exact framework of the quantum many-body problem. In practice, the accuracy of observables in DFT highly depends on the choice of the approximate xc-functional. From the local density approximation (LDA) [6], to the gradient expansions such as the generalized gradient approximations (GGAs), e.g. Perdew–Burke–Enzerhof [7] and the hybrid functionals such as B3LYP [8], to the orbital-functionals such as optimized effective potentials [9] and to the range-separated hybrids such as HSE06 [10], the last decades have seen great efforts and achievements in the development of functionals with more accurate and reliable prediction capability.

Nonetheless, available approximate functionals such as the LDA, the GGA's and the hybrid functionals have known shortcomings to model gaps of semiconductors [11], molecular dissociation curves [12], barriers of chemical reactions [13], polarizabilities of molecular chains [14, 15], and charge-transfer excitation energies, particularly between open-shell molecules [16].

Practical applications of density functional theory encounter two major problems: (i) while the Hohenberg–Kohn theorem tells us that arbitrary ground-state observables are functionals of the ground-state density, it does

not provide us with the explicit density functional dependence. (ii) Even for observables for which the exact expression of the density-functional is known, solely the true exact density gives back the exact properties of the system. Common xc-functionals fail to reproduce the exact density in the strong-correlation limit. Any deviations from the exact density directly translates to observables regardless whether the exact expression of the density functionals is used.

In this work, we explicitly illustrate the density functional dependence of arbitrary observables for a specific model system. This illustrates explicitly what was proven by Hohenberg and Kohn—but does not provide a general recipe how to derive the functional expression of arbitrary observables for other systems. Further, we illustrate problem (ii) by showing that the localization of the density directly manifests in the functional dependence of arbitrary observables.

Recent advances in functional development such as optimally tuned range separated functionals [17], ensemble density functional theory [18, 19] and local scaling corrections [20], logarithmically enhanced factors in gradient approximations [21] and the particle–particle random-phase approximation [22] can diminish or even cure some of the above mentioned shortcomings but not all of them.

Shortcomings of approximate functionals indicate that some important qualitative features of the exact functional are not (sufficiently well) captured. A common example is the delocalization error as in the case of stretched molecules, where approximate functionals such as LDA and GGA's tend to artificially spread out the ground-state electron density in space [23]. Since in DFT every observable is a functional of the ground-state density the delocalization error transmits into all observables as functional of the density and in particular to the ground-state energy functional. As a consequence most approximations for the ground-state energy as functional of the particle number N are either concave or convex functions between integer N's [20, 24] and hence, violate the exact Perdew–Parr–Levy–Balduz condition [25] which states that the ground-state energy as a function of the particle number $E(N)$ is a linear function between integer N. The linearity of $E(N)$ leads to the commonly known derivative discontinuity [25] and is one exact condition on the xc-functional. Exact conditions on the xc-functional are a very useful tool in the development of new, improved functionals. In this paper we discuss an exact condition on the xc-functional that is relevant for systems consisting of well separated but mutually interacting fragments, such as in stretched molecules. Among the approaches to model the limit of strongly correlated, low density systems with DFT we highlight the long range corrected hybrids [26], the generalization of the strictly correlated electron functional to fractional electron numbers [27–30] and the recently introduced local scaling correction, which imposes the linearity condition to local regions of the system, correcting both energies and densities and affirming the relevance of modeling fractional electron distributions to reduce the delocalization error [20].

Exactly solvable model systems have shown to provide useful insight essential to understand the failures of approximate xc-functionals and to develop new and improved approximations. For example, by studying one-dimensional model systems of few electrons it was shown that in the dissociation limit of molecules, the exact xc-potential as function of the spatial coordinate develops steps and peaks [31–37]. Such features are manifestations of strong-correlation and the absence of such features in approximate functionals results in delocalization errors. The correlation of molecules in the dissociation limit is usually dominated by static correlation, also known as near-degeneracy correlation. A good measure for the static correlation in the system is the von-Neumann entropy. It can be understood as well as a measure of the Slater rank [38, 39]. In the following, we refer to strongly correlated systems if the ground-state wavefunction is not well approximated by a single Slater determinant. Further, we do not allow spin-symmetry breaking.

Recently, [40–42] established an explicit connection between the xc potentials and the wave functions allowing to directly compute the xc potentials from the many-electron wave functions in a numerically robust manner. Studies of exact ground-state xc-functionals for lattice models include the exact one-to-one map between ground-state densities and potentials computed for a half-filled one-dimensional Hubbard chain in [43] using the Bethe Ansatz, for the one-site and double-site Hubbard models in full Fock space in [44, 45] and for the two-electron Hubbard dimer via constraint search in [46], among others. For such lattice models the Hohenberg–Kohn theorem [47] can be generalized by replacing the real-space potentials and densities by on-site potentials and on-site occupations [48, 49]. The finite Hilbert space of lattice models permits the construction of the exact density-to-potential map. The question arises what can be learned about realistic three-dimensional systems by studying one-dimensional lattice models. Recently it was shown [50, 51] that the time-dependent exact xc-functional of the one-dimensional Hubbard dimer in the strongly correlated limit develops the same step feature as the real-space one-dimensional model studied in [52]. The step feature in the real-space model in the strongly correlated limit is equivalent in the Hubbard dimer to a jump in the ground-state xc potential difference as a functional of the density difference δn between the two sites, $\delta v_{Hxc}[\delta n]$, as the strongly correlated limit is approached. The step saturates to the ionization potential difference between the two wells in the real space model [31–37] whereas in the dimer, the value of $\delta v_s[\delta n]$ saturates to δv, the external potential difference [50, 51]. Note, in contrast to [50, 51] where the electron–electron interaction is on-site Hubbard, in this work we

study lattice models with soft-Coulomb interaction between particles. Reference calculations of [53] show that one-dimensional model systems capture the essence of three-dimensional systems when studying strong-correlation in DFT.

In this work, we study the exact density-to-potential and density-to-wavefunction map of a one-dimensional lattice model with a system size that still allows to exactly diagonalize the Hamiltonian in full Fock space. The wavefunction-to-density map has been fully realized for fixed particle number, i.e. for the two-electron singlet case by [54, 55] and for the more-electron case by [56, 57]. In principle, a small system size of the model used in this work allows to graphically illustrate the complete density-to-wavefunction map in the full Fock space of the system, and can be used to show how features such as the intra-system steepening and the inter-system derivative discontinuity of the density-to-potential map appear in the density-to-wavefunction map. As example, we explicitly show the complete density dependence of the two-electron singlet ground-state wavefunction. For different values of the external potential in the Hamiltonian we perform exact diagonalization of the Hamiltonian. Each diagonalization gives us all eigenfunctions and eigenenergies of the system, where the eigenstate with lowest eigenenergy corresponds to the ground state. We use the ground-state of each exact diagonalization corresponding to a fixed external and fixed chemical potential to construct both one-to-one maps, i.e. the map between on-site potentials and ground-state on-site occupations (ground-state densities), and the map between ground-state densities and ground-state wave-functions. To illustrate the latter, we numerically construct the configuration-interaction (CI) coefficients of the wave-function expansion as functionals of the ground-state density. We study the exact features of these maps for systems with different ratio of discrete values of the kinetic hopping probability λ_t to the electron–electron interaction strength λ_w. This allows us to study the exact maps from the non-interacting to the strictly localized electron limit while we gradually change the correlation of the system. We illustrate how the distinctive features of the exact density-to-potential map transmit into the wavefunction-to-density map, and further into expectation values and transition matrix elements of *arbitrary* operators as functionals of the ground-state density.

We show that in approaching the limit of strongly correlated electrons, i.e. $\frac{\lambda_t}{\lambda_w} \rightarrow 0$, the gradient of the exact density-to-potential map of our model system steepens. We denote this feature as intra-system steepening which gradually builds up within the system as the hopping probability favoring the delocalization of electrons decreases and the electron–electron interaction favoring the localization increases. In the strictly localized electron limit, where $\lambda_t = 0$, we see that the ground-state becomes degenerate and hence, the intra-system steepening transforms into the step-like inter-system derivative discontinuity.

We find that qualitative features such as the intra-system steepening and the inter-system derivative discontinuity of the density-to-potential map are already captured by a two-site lattice model. In the case of a two-site model, each site can be regarded as a subsystem. With increasing distance between the subsystems, the hopping probability decreases and the localization of the electrons on each site increases. If the sites are infinitely apart and the subsystems are truly separated, the electrons are strictly localized on each site. We simulate the infinite separation in the two-site model by setting the hopping parameter in the kinetic operator λ_t strictly to zero. Since the kinetic energy is strictly zero, this limit is a classical limit. However, setting λ_t equal to zero allows us to imitate the infinite bond-stretching of the molecular model, where the distance of the molecular wells d goes to ∞. In this limit, $\lambda_t = 0$ implying $d \rightarrow \infty$, the intra-system steepening of the density-to-potential map becomes the standard step-like inter-system derivative discontinuity.

Arbitrary observables and transition-matrix elements are affected by the presence of the intra-system steepening and the inter-system derivative discontinuity, and in particular by the lack of it in approximate functionals. We illustrate how both features are transmitted to the ground- and excited-state energy, the excited- and transition-state density and to the correlation entropy functionals.

The paper is organized as follows. In section 2 we present the exact maps between local potentials, ground-state wavefunctions and ground-state densities. In section 3 we introduce the lattice model and the methodology that we employ in the present work. Section 4 is dedicated to the study of the intra-system steepening of the exact one-to-one density-to-potential map when approaching the strictly localized limit (i.e. the strongly correlated limit) and its transition into a step function with only allowed discrete integer density values for truly separated subsystems. In section 4.1, we discuss how theses discrete integer density values of the decoupled systems connect if a weak coupling between the systems is introduced. In section 5 we use the potential-to-density map to construct the CI coefficients of the ground- and excited-state wavefunction expansions as explicit functionals of the ground-state density. Ground-state degeneracies leave topological scars in the electron density [58]. We illustrate how these degeneracies and furthermore also near-degeneracies of the eigenenergies of the system affect the ground- and excited-state expectation values and transition matrix elements of relevant operators as functionals of the ground-state density. Finally, in section 6, we summarize our findings and give an outlook for future work.

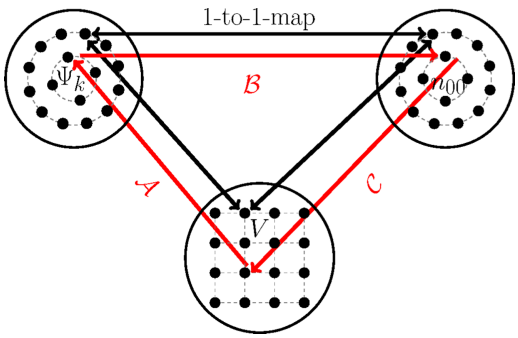

Figure 1. Schematic illustration of the exact mapping between N-electron wavefunctions Ψ_k, local potentials V, and ground-state electron densities n_{00}. The maps are depicted as red arrows, where $\mathcal{A}$ maps V onto Ψ_k, $\mathcal{B}$ maps Ψ_k onto n_{00} and $\mathcal{C}$ maps n_{00} onto V. Black arrows indicate the bijectivity of each of these one-to-one maps. Note that every element in V has an exact one-to-one equivalent in n_{00} and Ψ_0.

2. Exact mappings

To understand which features approximate functionals are missing, it is instructive to explicitly construct and to analyze the exact maps between the ground-state wavefunction Ψ_0, the local potential V, and the ground-state density n_{00}, sketched in figure 1. For fixed electron–electron interaction $\hat{W}$, the many-body Schrödinger equation

$$(\hat{T} + \hat{W} + \hat{V})\Psi_k = E_k\Psi_k, \tag{1}$$

defines a unique map between the set of local potentials V and the set of energy eigenstates Ψ_k, depicted as map $\mathcal{A}$ in figure 1. The ground-state density n_{00} can be computed as usual according to

$$n_{00}(\vec{r}) = N\int \mathrm{d}\vec{r}_2 ... \mathrm{d}\vec{r}_N\ |\Psi_0(\vec{r}_2 .., \vec{r}_N)|^2, \tag{2}$$

which establishes a unique map from the set of N-electron ground-state wavefunctions Ψ_0 to the set of N-electron ground-state densities n_{00}. Hohenberg and Kohn [47] proved that the map $\mathcal{C}$ in figure 1 between n_{00} and V is one-to-one and unique if V-representability is fulfilled [59–63]. Assuming existence of this one-to-one density-to-potential map allows in principle to construct any ground-state observable as a unique functional of the ground-state density n_{00},

$$O_{00}[n_{00}] = \langle\Psi_0[n_{00}]|\hat{O}|\Psi_0[n_{00}]\rangle. \tag{3}$$

Note that in addition to the one-to-one V-to-n_{00} map, the Schrödinger equation establishes a map between n_{00} and the excited-state wavefunctions Ψ_k, $k \neq 0$. As a consequence, excited-state expectation values with $k = l > 0$, and transition matrix elements with $k \neq l$, can be computed as functionals of the ground-state density using

$$O_{kl}[n_{00}] = \langle\Psi_k[n_{00}]|\hat{O}|\Psi_l[n_{00}]\rangle. \tag{4}$$

The ground-state energy E_0 and the ground-state density n_{00} can be accessed using the variational principle

$$E_0 = \min_n E_V[n], \quad E_0 < E_V[n], \quad n \neq n_{00}. \tag{5}$$

Given an external potential V the total energy is computed as $E_V[n] = F_{\mathrm{HK}}[n] + \int n(\vec{r})V(\vec{r})\mathrm{d}^3r$. In the Levy–Lieb constrained search formulation [64, 65] the Hohenberg–Kohn energy functional F_{HK} is found as the minimum over all possible N-electron densities n, of the expectation value of kinetic plus electron–electron interaction operator

$$F_{\mathrm{HK}}[n] = \min_{\Psi\to n}\langle\Psi[n]|\ \hat{T} + \hat{W}\ |\Psi[n]\rangle. \tag{6}$$

In the following, we illustrate the features of the exact density-to-potential and density-to-wavefunction maps explicitly for our model systems.

3. Lattice model

In the present work, we restrict ourselves to one-dimensional lattice systems for which the construction of exact functionals via exact diagonalization is numerically feasible. On a lattice, the potential becomes an on-site

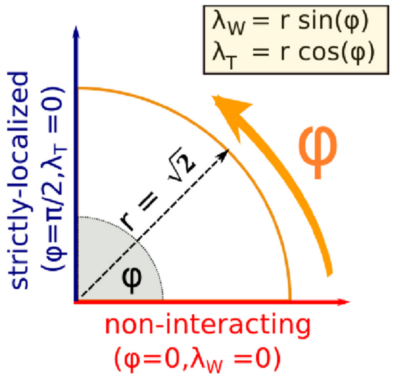

Figure 2. Illustration of the kinetic hopping probability λ_t and the strength of electron–electron interaction λ_w in polar representation for the lattice Hamiltonian used in this work as defined in equation (7).

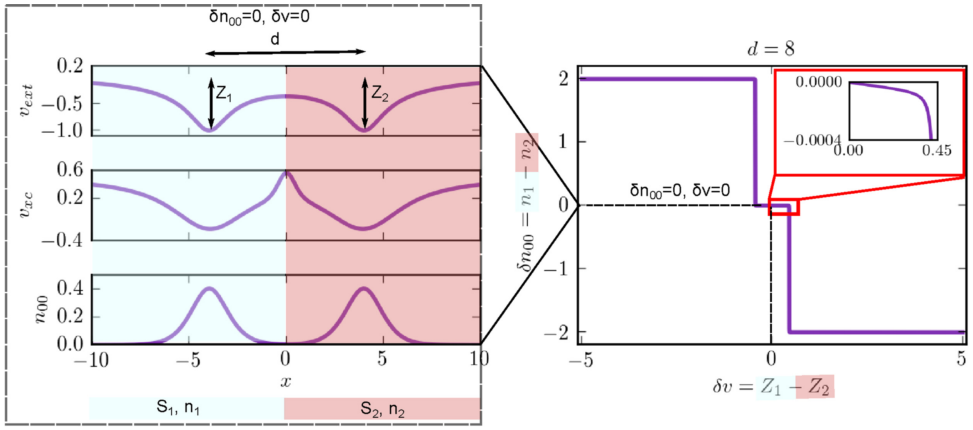

Figure 3. Sketch of Bader partitioning. Left panel from top to bottom: external potential for a one-dimensional diatomic molecule with nuclear charges $Z_1 = -1$ and $Z_2 = -1$ and atomic separation $d = 5$ a.u. and the corresponding exact exchange-correlation potential and ground-state density in real-space. We denote the blue-colored left halfspace as system S_1 and the red-colored right halfspace as system S_2. With increasing distance d of the molecular wells the coupling of both systems decreases. Figure on the right-hand: exact effective density-to-potential map, where we vary the potential difference $\delta v = Z_1 - Z_2$ from -5 to 5. The density difference δn_{00} corresponds to the electronic density summed over the left half-space minus the density summed over the right half-space as defined in equation (20). The point at ($\delta n_{00} = 0$, $\delta v = 0$) in this effective map corresponds to the three panels in real-space on the left-hand side. The red-framed zoom at the top corner shows that the density-to-potential map has a smooth behavior on the scale of the coupling of both systems.

potential $V(x) \rightarrow v(x_i)$, the density a site-occupation, $n(x) \rightarrow n(x_i)$, and the integral becomes a sum over sites i, $\int \mathrm{d}x \rightarrow \sum_i$ [48]. Furthermore, the kinetic energy operator becomes a nearest-neighbor hopping term.

3.1. Lattice Hamiltonian

For N interacting electrons in one spatial dimension we consider Hamiltonians of the form

$$\hat{H}^{\varphi} = \hat{H}(\varphi) = \lambda_t(\varphi)\hat{T} + \lambda_w(\varphi)\hat{W} + \hat{V} + \mu\hat{N}, \tag{7}$$

where the parameter μ, connected to the particle number operator $\hat{N}$, acts as a Lagrange multiplier shifting the state with lowest energy to blocks with different particle number N in Fock space. To switch between different coupling limits, we introduce the amplitude of the kinetic hopping $\lambda_t = r\cos(\varphi)$ and the strength of the electron–electron interaction $\lambda_w = r\sin(\varphi)$ as parameters in polar representation with radius r and angle φ, see figure 2. The limit $\lambda_w \rightarrow 0$, i.e. $\varphi = 0$, corresponds to non-interacting electrons and the limit $\lambda_t \rightarrow 0$, i.e. $\varphi = \frac{\pi}{2}$, to site-localized electrons. Without loss of generality we choose $r = \sqrt{2}$ and $\varphi \in \left[0, \frac{\pi}{2}\right]$. Throughout this work we use atomic units $\hbar = m = e = 1$.

Next, we introduce the operators of the lattice model with M sites and lattice spacing dx. In second-order finite difference representation the kinetic energy operator with nearest neighbor hopping $t_0 = \frac{1}{\mathrm{d}x^2}$ reads

$$\hat{T} = -\frac{t_0}{2}\sum_{l=1}^{M}\sum_{\sigma}\hat{c}^{\dagger}_{l,\sigma}\hat{c}_{l+1,\sigma} + \hat{c}^{\dagger}_{l+1,\sigma}\hat{c}_{l,\sigma} - 2\hat{c}^{\dagger}_{l,\sigma}\hat{c}_{l,\sigma}, \tag{8}$$

where $\hat{c}^{\dagger}_{l,\sigma}$ and $\hat{c}_{l,\sigma}$ denote creation and annihilation operators of an electron placed on site l with spin projection onto the z-axis σ. Usually, the hopping t_0 changes with the lattice spacing dx. However, we choose to leave dx fixed and use the parameter λ_t and λ_w instead. The last term in equation (8) corresponds to on-site hopping. For model systems this term is usually not taken into account. Here we keep the term to allow for a consistent first and second quantized treatment of the Hamiltonian. We study the non-local soft-Coulomb electron–electron interaction

$$\hat{W}_{\mathrm{SC}} = \sum_{l,m,\sigma,\sigma'}\frac{\hat{c}^{\dagger}_{l,\sigma}\hat{c}^{\dagger}_{m,\sigma'}\hat{c}_{m,\sigma'}\hat{c}_{l,\sigma}}{2\sqrt{(\mathrm{d}x\,(l-m))^2 + a}}, \tag{9}$$

acting on particles located at sites l and m with spins σ and σ'. Throughout this work the Coulomb interaction is softened by the parameter $a = 1$. The external potential

$$\hat{V} = \sum_{l=1}^{M} v_l \hat{c}^{\dagger}_{l}\hat{c}_{l}, \tag{10}$$

introduces a potential difference between the sites in the lattice, which depending on its strength, shifts the electron density among the sites in the lattice. We restrict ourselves to two different scenarios for which exact diagonalization is still possible, similar to [66, 67]. In case (i) we consider two spin-singlet electrons on $M = 206$ sites. The particles are confined in a box from $x = -10.25$ a.u. to $x = +10.25$ a.u. with zero boundary conditions and a lattice spacing of d$x = 0.1$ a.u. and $\lambda_t = \lambda_w = 1$. To mimic the bond-stretching in molecular systems, we consider an external potential

$$v_l = \frac{Z_1(\alpha)}{\sqrt{\left(x_l - \frac{d}{2}\right)^2 + 1}} + \frac{Z_2(\alpha)}{\sqrt{\left(x_l + \frac{d}{2}\right)^2 + 1}} + \frac{Z_1(\alpha)Z_2(\alpha)}{\sqrt{(d^2+1)}}, \tag{11}$$

$$Z_1(\alpha) = -\alpha, \quad Z_2(\alpha) = -(2-\alpha) \tag{12}$$

with two atomic wells separated by distances ranging from $d = 2$ to $d = 8$ a.u.. The depth of the wells is given by the nuclear charges Z_1 and Z_2 which we modulate with the parameter $\alpha \in [0,\ 2]$. We will see that the essence of such a system is already captured by a two-site model. As case (ii), we consider $M = 2$ sites in the lattice with a distance d$x = \frac{1}{\sqrt{2}}$, where we vary the parameters λ_t and λ_w. In this case, the system size allows to perform exact diagonalization in the full Fock space of the model.

3.2. Methodology

To explicitly construct the one-to-one map between external potentials and ground-state densities, we diagonalize the Hamiltonian introduced in equation (7) for different external potentials v_m, but fixed φ. The external potential takes values $v_m = m\Delta_v$, where Δ_v is the numerical step size, and m is the step number. Although not shown in the present work, similarly the Hamiltonian can be diagonalized for different chemical potentials μ_k with the chemical potential values $\mu_k = k\Delta_\mu$, the numerical step size Δ_μ and the step number k. In this way all functionals are constructible as functions of the particle number N and can be studied in complete Fock-space. Here we fix the chemical potential and select a discrete and uniformly distributed set of potentials from the continuous set V of possible external potentials in figure 1. In the next step we use exact diagonalization to compute the ground-state wavefunction Ψ^{φ}_0 and energy E^{φ}_0 corresponding to each value of v_i and μ_i (but fixed φ). For each ground-state wavefunction, we compute the corresponding on-site ground-state density

$$n^{\varphi}_{00}(x_j) = \langle\Psi^{\varphi}_0|\ \hat{n}(x_j)|\Psi^{\varphi}_0\rangle, \tag{13}$$

where j is the site subindex, and the spin-summed density operator reads

$$\hat{n}(x_j) = \hat{c}^{\dagger}_{j,\uparrow}\hat{c}_{j,\uparrow} + \hat{c}^{\dagger}_{j,\downarrow}\hat{c}_{j,\downarrow}. \tag{14}$$

In addition to the ground-state wavefunction, the exact diagonalization gives us access to the excited-state wavefunctions $\Psi^{\varphi}_{k\neq 0}$, which allows us to compute excited-state observables and transition matrix elements of operators as functionals of the ground-state density according to equation (4). On a lattice with M sites, the continuous one-dimensional ground-state density $n_{00}(x)$ becomes a vector $(n_{00}(x_1),\ n_{00}(x_2),\ldots,\ n_{00}(x_M))$. Hence, expectation values and transition matrix elements as functionals of the density become rank M tensors

$$O^{\varphi}_{kl}(n_{00}(x_1),\ldots,n_{00}(x_M)) = \langle\Psi^{\varphi}_k(n_{00}(x_1),\ldots,n_{00}(x_M))|\hat{O}|\Psi^{\varphi}_l(n_{00}(x_1),\ldots,n_{00}(x_M))\rangle. \tag{15}$$

In case (ii) where two sites in the lattice are considered, all functionals depend on the on-site densities $n_{00}(x_1)$ and $n_{00}(x_2)$, i.e. $|\Psi^{\varphi}_k[n_{00}(x_1),\ n_{00}(x_2)]\rangle$ and $V^{\varphi}[n_{00}(x_1),\ n_{00}(x_2)]$. Instead of expressing all functional dependencies in terms of the variables $n_{00}(x_1)$ and $n_{00}(x_2)$, we rotate the coordinate system to the total particle number

$N = n_{00}(x_1) + n_{00}(x_2)$ and the occupation difference $\delta n_{00} = n_{00}(x_1) - n_{00}(x_2)$ between the sites [46]. To illustrate the wavefunction-to-density map, we expand the ground ($k = 0$) and the excited ($k > 0$) eigenstates $|\Psi_k^\varphi\rangle$ of the system in a complete set of Slater determinants $|\Phi_q\rangle$,

$$|\Psi_k^\varphi[\delta n_{00}, N]\rangle = \sum_q \alpha_q^{\varphi,k}[\delta n_{00}, N]|\Phi_q\rangle, \tag{16}$$

where we have chosen $|\Phi_q\rangle$ to be the eigenstates of the kinetic operator $\hat{T}$. This gives rise to the CI coefficients

$$\alpha_q^{\varphi,k}[\delta n_{00}, N] = \langle\Phi_q|\Psi_k^\varphi[\delta n_{00}, N]\rangle. \tag{17}$$

By writing the CI-coefficients $\alpha_q^{\varphi,k}[\delta n_{00}, N]$ as explicit functionals of δn_{00}, we gain access to all ground- and excited-state expectation values or transition matrix elements of any operator, i.e.

$$\begin{aligned} O_{kl}^\varphi[\delta n_{00}, N] &= \langle\Psi_k^\varphi[\delta n_{00}, N]|\ \hat{O}\ |\Psi_l^\varphi[\delta n_{00}, N]\rangle \\ &= \sum_q\sum_{q'} \alpha_{q'}^{\varphi k *}[\delta n_{00}, N]\alpha_q^{\varphi l}[\delta n_{00}, N]\langle\Phi_{q'}|\ \hat{O}\ |\Phi_q\rangle. \end{aligned} \tag{18}$$

A prime example is the Hohenberg–Kohn energy functional defined in equation (6), which is the ground-state expectation value of the Hamiltonian $\hat{H}_{v_l=0}^\varphi = \lambda_t(\varphi)\hat{T} + \lambda_w(\varphi)\hat{W}$, i.e.

$$\begin{aligned} F_{00}^\varphi[\delta n_{00}, N] &= \langle\Psi_0^\varphi[\delta n_{00}, N]|\ \hat{H}_{v_l=0}^\varphi\ |\Psi_0^\varphi[\delta n_{00}, N]\rangle \\ &= \sum_{q,q'} \alpha_q^*[\delta n_{00}, N]\alpha_q[\delta n_{00}, N]\langle\Phi_{q'}|\ \hat{H}_{v_l=0}^\varphi\ |\Phi_q\rangle. \end{aligned} \tag{19}$$

For the two-particle singlet states, we compute the Hohenberg–Kohn functional for different values of $\varphi \in \left[0, \frac{\pi}{2}\right]$. Note the explicit dependence of $F_{00}^\varphi[\delta n_{00}, N]$ on the angle φ, since the Hohenberg–Kohn proof can only be established for fixed and given kinetic energy and particle–particle interaction. By changing the angle φ, we construct the exact energy functional $F_{00}^\varphi[\delta n_{00}, N]$ for different electron–electron interactions and kinetic terms, where $\varphi = 0$ is the non-interacting and $\varphi = \frac{\pi}{2}$ the infinitely correlated limit. Our approach allows to construct the exact density functionals for any observable of interest. We illustrate this for a few selected examples in the following sections. Also we emphasize that throughout this work all functionals are constructed in the zero-temperature limit.

4. Features of the exact density-to-potential map

We start our analysis for the Hamiltonian of case (i), where we consider a diatomic molecule with different interatomic separations. While the full density-to-potential map is a high-dimensional function for $M = 206$ sites and impractical to visualize, the essence of the bond stretching can be captured by the integrated densities of fragments of the system. A natural choice to partition the system into its fragments, is to divide the total molecular charge distribution at its minima into different Bader basins [68, 69]. By integrating the density over each of these Bader basins, the high dimensionality of the density in real-space reduces drastically. For our diatomic model the partitioning reduces the dimensionality from 206 to two, by mapping the sites in the grid onto the basins. We can then refer to each basin as a *effective site* in real space and regard the density difference between the basins as density difference between the two sites. For the simple diatomic molecule in one-dimension, we simply divide the system in two equal half-spaces, and construct the density-difference according to

$$\delta n_{00} = \sum_{i=1}^{M/2} n_{00}(x_i) - \sum_{i=M/2+1}^{M} n_{00}(x_i). \tag{20}$$

To obtain the potential difference between the two basins, we take the difference between the maximum depth of the molecular potential wells of each basin and define the potential difference as $\delta v = Z_1(\alpha) - Z_2(\alpha)$. Note, the potential difference can be tuned by changing the nuclear charge of the two atoms with the parameter α of equation (12). The resulting *effective* density-to-potential map for our diatomic model is shown in figure 4. Starting from left to right we increase the distance between the molecular wells. The effective density-to-potential map starts out with a smooth monotonic shape. When the distance of the atoms is increased the gradient of the effective density-to-potential map steepens, leading ultimately to steps in the density values for the infinitely separated limit.

The very same qualitative behavior can be found for a simple two-site lattice system. As a second example we consider therefore the Hamiltonian of case (ii). In this case we construct the exact density-to-potential map for the two-particle singlet states of the two-site lattice model. The results are shown in figures 5 and 6. Figure 5 shows the Hartree exchange-correlation part of the exact potential as functional of the ground-state density, whereas the first row of figure 6 shows the dependence of the exact density as function of the external potential

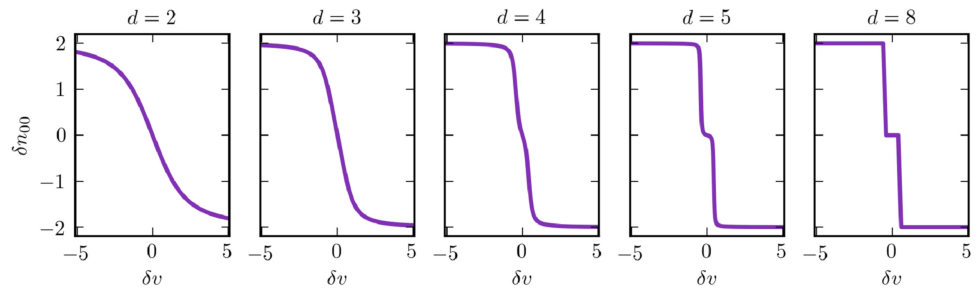

Figure 4. Exact density-to-potential map for a one-dimensional diatomic molecule with nuclear charges Z_1 and Z_2, where we vary the potential difference $\delta v = Z_1 - Z_2$ from -5 to 5 for different atomic separations $d = 2 - 8$ a.u. similar to [66, 67]. The density difference δn_{00} corresponds to the electronic density summed over the left half-space minus the density summed over the right half-space as defined in equation (20) and illustrated in figure 3. The graph illustrates the influence of electron localization on the ground-state density-to-potential map. From left to right the distance of the molecular wells increases while the gradient of the density-to-potential steepens with increasing distance d and hence, decreasing coupling of the fragments of the system. We denote this feature of the density-to-potential map as intra-system steepening (see text for details).

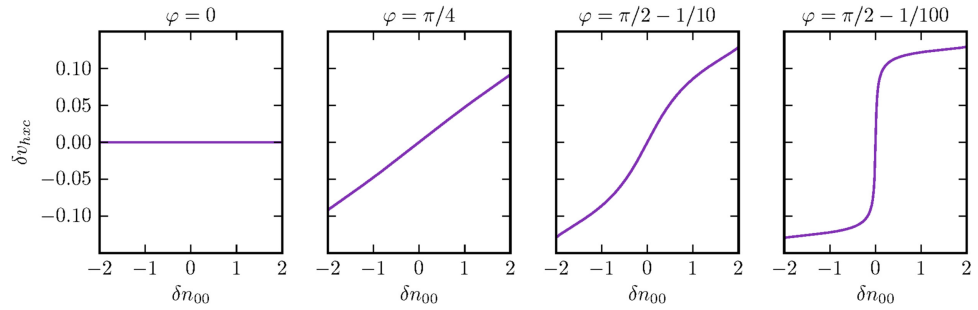

Figure 5. Exact Hartree exchange-correlation potential calculated with the exact formula of [37] as functional of the ground-state density for a two-site lattice model using soft-Coulomb interaction. From left-to-right we approach the strictly localized limit. Note, in contrast to figures 4 and 6, here we show the inverse map δv_{hxc}-to-δn_{00} by swapping the x- and y-axis.

difference between the sites. Note the density-to-potential map in figure 6 is one-to-one, and therefore invertible, the domain and co-domain of the selected independent variable and the corresponding function values can be swapped. In addition to the ground-state density-to-potential map in the first row of figure 6, the second and the third row show the first and the second excited-state density-to-potential map, and the fourth row shows the eigenenergies E_0, E_1 and E_2 as function of the external potential difference between the two sites in lattice. From left to right, φ increases, i.e. the electron–electron interaction favoring the localization of the electrons increases, whereas the kinetic energy favoring the delocalization decreases, i.e. $\frac{\lambda_t}{\lambda_w} \to 0$. This localization is reflected by the steep gradient of the ground- and excited-state densities δn_{00}, δn_{11} and δn_{22} as function of the external potential difference $\delta v = v_1 - v_2$. For the potential difference we select values from -5 to 5, shifting the electron density from one site in the lattice to the other. Setting $\varphi = 0$ in equation (7) corresponds to non-interacting electrons, where the eigenfunctions are single-particle Slater-determinants. In this limit the density-to-potential map for our model can be found analytically

$$\delta n_{00}^{\varphi=0}(\delta v,\, \lambda_t,\, \mathrm{d}x) = -\frac{4\mathrm{d}x^2\delta v}{\sqrt{4\mathrm{d}x^4\delta v^2 + \lambda_t^2(\varphi = 0)}}. \tag{21}$$

The map behaves smoothly as can be seen in the leftmost figure in the first row of figure 6.

Approaching the strictly localized limit, i.e. $\varphi \to \frac{\pi}{2}$, the slope of the exact density-to-potential map sharpens until the map develops a characteristic feature, which we denote as intra-system steepening. The intra-system steepening of the gradient of the density-to-potential map corresponds to the localization of the electrons in the respective subsystems. Near the strictly localized limit, e.g. $\varphi = \frac{\pi}{2} - \frac{1}{100}$, the electrons are highly localized on the sites.

In the strictly localized electron limit $\varphi = \frac{\pi}{2}$ the hopping parameter is equal to zero. In this limit the system 'breaks' into two kinetically decoupled sites and the Hamiltonian reduces to $\hat{H}^{\varphi=\frac{\pi}{2}} = \hat{W} + \hat{V}$ and hence commutes with the position operator $\hat{x} = \sum_{m=1}^{M}\sum_{\sigma} x_m \hat{c}_{m,\sigma}^{\dagger}\hat{c}_{m,\sigma}$ with $x_m = -(M+1)/2\mathrm{d}x + m\mathrm{d}x$.

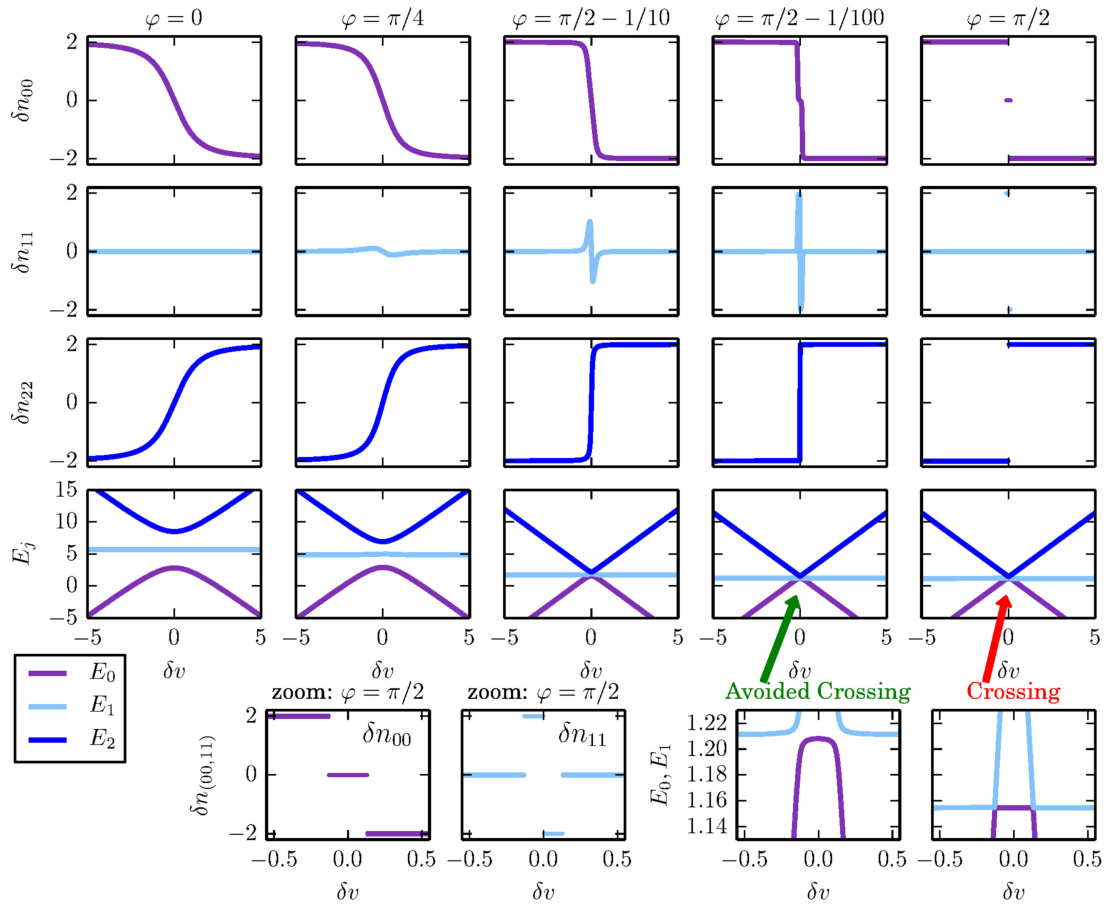

Figure 6. Exact density-to-potential map for a two-site lattice model using soft-Coulomb interaction. Despite its reduced dimensionality essential features of the density-to-potential map of the molecular model system are already captured by a two-site model, as can be seen by comparing figures 4 and 6. The graphs illustrate how the electron localization is captured in the ground- and excited-state density-to-potential maps and in the eigenenergies. Upper panel: exact ground-state density as function of the external potential, i.e. $\delta n_{00}(\delta v)$. Second panel: exact first excited-state density as function of the external potential, i.e. $\delta n_{11}(\delta v)$. Third panel: exact second excited-state density as function of the external potential, i.e. $\delta n_{22}(\delta v)$. Lower panel: eigenenergies of the two-particle singlet states as function of the external potential $E_j(\delta v)$, where E_j corresponds to the eigenstate $|\Psi_j\rangle$ and to the density differences $\delta n_{jj} = \langle\Psi_j|\ \delta\hat{n}\ |\Psi_j\rangle$. Inset at the bottom on the left-hand side: detailed view of the ground-state and the first excited-state density functionals $\delta n_{00}(\delta v)$ and $\delta n_{11}(\delta v)$ in the strictly localized limit. Inset at the bottom at the right-hand side: avoided and real crossings of eigenenergies. From left to right the angle φ increases the correlation in the system going from the non-interacting ($\varphi = 0$) to the strictly site-localized electron limit $\left(\varphi = \frac{\pi}{2}\right)$. In the molecular model system of figure 4 this corresponds to an increasing distance d of the molecular wells. The gradient of all three densities steepens whenever the corresponding eigenstate as functional of the external potential comes close to an avoided crossing. We denote this exact feature of the density-to-potential map as intra-system steepening. In the strictly localized limit $\left(\varphi = \frac{\pi}{2}\right)$ the intra-system steepening becomes the inter-system derivative discontinuity while the avoided crossing turns into a real-crossing with degenerate eigenenergies.

$$[\hat{H}^{\varphi=\frac{\pi}{2}}, \hat{x}] = 0, \tag{22}$$

and the eigenfunctions of $\hat{H}$ are diagonal in the eigenbasis of the position operator. The three two-particle singlet states correspond to the physical situations where both electrons are located on site one, i.e. $\left|\Psi_0^{\varphi=\frac{\pi}{2}}[\delta n_{00} = +2]\right\rangle = \hat{c}_{1\downarrow}^\dagger \hat{c}_{1\uparrow}^\dagger\ |0\rangle$, both electrons are on site two, i.e. $\left|\Psi_0^{\varphi=\frac{\pi}{2}}[\delta n_{00} = -2]\right\rangle = \hat{c}_{2\downarrow}^\dagger \hat{c}_{2\uparrow}^\dagger\ |0\rangle$, or where the electrons are delocalized over both sites, i.e. $\left|\Psi_0^{\varphi=\frac{\pi}{2}}[\delta n_{00} = 0]\right\rangle = \frac{1}{\sqrt{2}}(\hat{c}_{1\downarrow}^\dagger \hat{c}_{2\uparrow}^\dagger - \hat{c}_{1\uparrow}^\dagger \hat{c}_{2\downarrow}^\dagger)|0\rangle$. Depending on the ratio between the external potential difference δv and the electron–electron repulsion strength λ_w, (except in the points of degeneracy) one of these three eigenstates is energetically more favorable and becomes the ground-state of the electronic system, see lower panel of figure 6. In the strictly localized limit, the density difference δn_{00} transitions from a continuous variable to a *discrete set* of integer values. Namely, the only possible values for the ground-state density differences are the integer values

$$\delta n_{00}^{\varphi=\frac{\pi}{2}}(\delta v) = \begin{cases} -2, \\ 0, \\ +2. \end{cases}$$

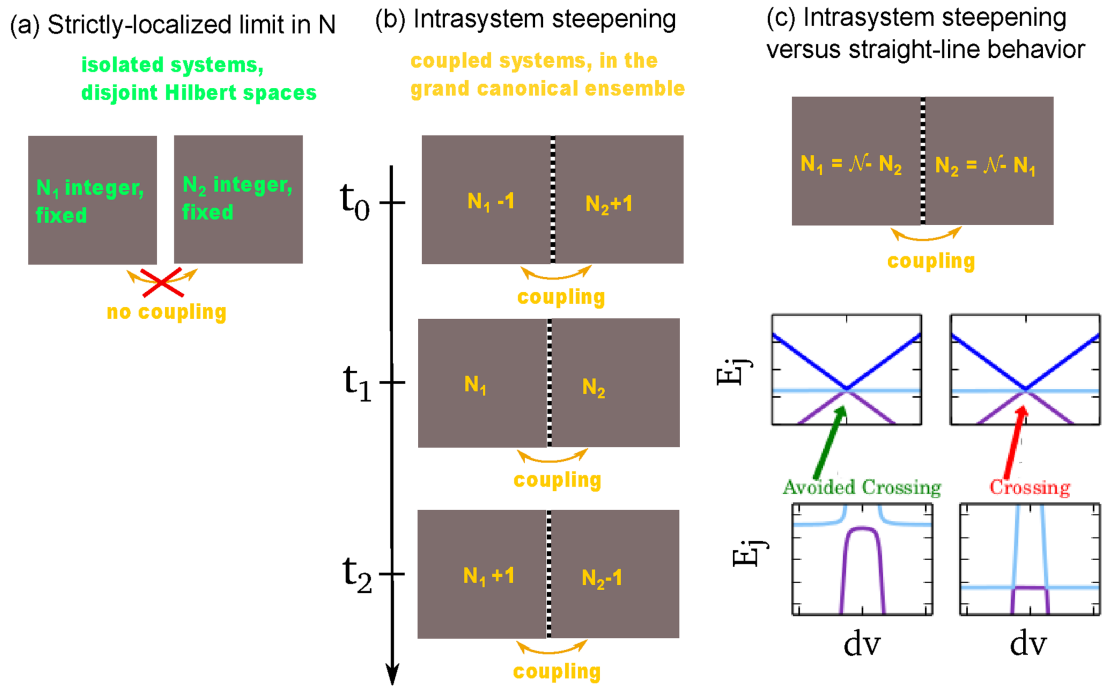

Figure 7. Differences between the strictly localized limit (a), the intra-system steepening (b), (c) and the inter-system derivative discontinuity (c), see discussion in section 4.1. Note, all three cases are mathematically well-defined limits. However, limit (a) and in general also the inter-system derivative discontinuity of limit (c) (except for an accidental degeneracy of the ground-state) are purely mathematically constructions, whereas processes in nature happen in the limit of (b) since neither the kinetic coupling nor the particle interaction can be fully switched off. We consider two systems S_1 with particle number N_1 and S_2 with particle number N_2. In figure (a) both systems are decoupled, and the ground-state of each isolated system is a pure state with fixed, integer particle number leading to a distributional density-to-potential map. The Hohenberg–Kohn theorem is valid in the disjoint Hilbert space of system S_1 and S_2, but not in the combined Hilbert space of both systems. Figure (b) shows the time-evolution of the system S_1 with initially $N_1 - 1$ particles to $N_1 + 1$. The particle number of system S_1 can only change if the system is coupled to a bath, here system S_2 with initially $N_2 + 1$ particles. Figure (c) shows the eigenenergies of the two-particle singlet states as in figure 6 and illustrates the difference between the intra-system steepening and the inter-system derivative discontinuity. The question is how the functionals of the densities of system S_1 and S_2 in figure (a) connect if a weak coupling between the systems is introduced. Note, although in the two-site model we kinetically decouple both sites, the sites are still coupled via the long-range soft-Coulomb interaction. For an accidental degeneracy of the ground-state, functionals are constructible as linear combination of the degenerate subspace. This construction then leads to the well-known straight-line behavior along the cut in the variable N of ground-state density functionals which are not differentiable at integer particle number $\mathcal{N} = N_1 + N_2$. In general a weak coupling lifts the degeneracy of the ground-state of the system as indicated on the bottom of the figure and leads to a smooth density-to-potential map. The gradient of this map steepens with decreasing coupling of the systems. The intra-system steepening is valid from strong to weak coupling.

For fully decoupled systems the different values of the external potential lead to the same density difference δn_{00} as can be seen in the map for $\varphi = \frac{\pi}{2}$ in figure 6. Therefore, the one-to-one map between δn_{00} and δv breaks down. The Hohenberg–Kohn theorem is applicable to each disjoint system but not to the combined system. For $\varphi = \frac{\pi}{2}$, the two sites kinetically decouple, however both sites are still coupled via the long-range soft-Coulomb interaction. For zero kinetic coupling, the ground-state of this combined system becomes degenerate in two points near $\delta v = 0$. Due to the points of degeneracy of the ground-state of the system, the distributional points of the density-to-potential map can be connected via straight-lines and the intra-system steepening transitions into the inter-system derivative discontinuity. Consequently, functionals along the cut in the variable δn are a linear combination of the functionals of the degenerate densities as has been shown for the ground-state energy functional as functional of the particle number[25, 70]. Therefore, we connect the distributional points along the variable δn for all functionals via straight lines, i.e. $\delta n_{00} = \pm 2(1 - \omega)$ and $0 \leqslant \omega \leqslant 1$. In a physical picture each one of the kinetically disconnected sites can be seen as a system infinitesimally weakly connected to a grand-canonical particle reservoir.

Contrary to the widely discussed inter-system derivative discontinuity, which describes the piece-wise linear behavior of the energy as a function of the particle number $E[N]$, the intra-system steepening describes the smooth behavior of the energy as functional of the density difference between fragments *within* the system $E[\delta n_{00}]$. Both features already show up in the density-to-potential map and transmit to all observables. The Hohenberg–Kohn energy functional is therefore only one specific example for the appearance of the inter-system derivative discontinuity and the intra-system steepening. The smooth behavior of the intra-system steepening is a consequence of the mixing of different quantum eigenstates around avoided crossings, and the steps related to the inter-system derivative discontinuity directly result from intersections of eigenenergies, thus

real crossings, see lower panel and inset of figure 6. The inter-system derivative discontinuity appears when electrons are strictly localized in states with different particle number but an accidental degeneracy of the ground-state allows the statistical mixture of the degenerate ground-states. Note that the steepening of the gradient for δn_{00} as well as for δn_{11} and δn_{22} arises whenever the eigenvalues of the Hamiltonian in equation (7) as function of the external potential become nearly degenerate. The connection between the avoided crossing and the steepening of the gradients functional is closely related to the finding of [36], i.e. that the step feature of the exact xc-potential in space arises in the vicinity of the avoided crossing, when the bonding and antibonding orbitals become nearly degenerate. Without this step feature (and the peaks) of the exact xc-potential, the non-interacting electron density would artificially smear out over both basins and lack the intra-system steepening of the exact electron density-to-potential map. For $\varphi = 0$ all eigenvalues are non-degenerate, hence the density-to-potential map of all eigenstates behaves smoothly. When we approach the strongly correlated limit at $\varphi \to \frac{\pi}{2}$, the first and second excited-state energies approach each other $E_1[\delta v] \to E_2[\delta v]$ and for $\varphi = \frac{\pi}{2}$ they become degenerate for $\delta v = 0$, i.e. $E_1[\delta v] = E_2[\delta v]$ (see inset figure 6). Because of this degeneracy of the first and second excited-state, the distributional points $+2$ and -2 of the first and second excited-state density as functional of the ground-state density can be connected via straight lines along the cut in the variable δn, see also figure 10. Caused by a real crossing of the eigenenergies in the strictly localized limit, the one-to-one correspondence with an external potential breaks down for all densities, i.e. the ground-state and the excited-state densities. The density-to-potential map becomes a distribution in this limit and the Hohenberg–Kohn theorem does not apply.

4.1. Intra-system steepening versus intersystem derivative discontinuity

In DFT, the ground-state wavefunction and all ground-state observables are unique functionals of the ground-state density. In this work, we also show the functional behavior of excited-state observables and transition matrix elements, for which in general no one-to-one correspondence exist. Nevertheless, as we will see in the following sections, features of the exact density-to-potential map directly translate to both types of functionals, i.e. the unique ground-state functionals and the generally non-unique functionals of the excited-state observables and the transition matrix elements. Therefore, it is of fundamental importance to identify and classify these features of the exact density-to-potential map. In the following, we distinguish between the three different cases displayed in figure 7. For all cases let us assume, that we have two systems S_1 and S_2. In the two-site lattice model one site corresponds to S_1 and one to S_2, whereas in the many-site model one basin corresponds to S_1 and the other one to S_2. In the first case as in figure 7(a) the kinetic coupling as well as the coupling via electron–electron interaction between the systems are strictly zero. This is a purely mathematical limit, since each system S_1 and S_2 is completely isolated from its environment and thus, the particle number in the system can not change. The Hilbert space of both systems is disjoint. The ground-state of each system corresponds to a pure state with fixed particle number. The Hohenberg–Kohn theorem is valid in the Hilbert space of each system, but not in the combined Hilbert space of both decoupled systems S_1 and S_2. The cut along δn_{00} of the density-to-potential map of the total system is a step function, where the values of δn_{00} are the particle number of system S_1 and S_2, i.e. N_1 and N_2. For fully decoupled systems S_1 and S_2, the functionals of this step-like density-to-potential map can only take values at the integer particle number of system S_1 and S_2, i.e. $F[N_1 \text{ and } N_2]$, where the values of the functional at N_1 and N_2 are disconnected. In the second case displayed in figure 7(b) the coupling of the systems ranges from strong to infinitesimally weak. Without loss of generality, we refer to S_1 as system and to S_2 as bath. This case is the underlying concept of charge transfer processes or in the description of band gaps of a system, where the particle number is changed by adding or removing a particle. These processes are not instantaneous processes, but should be regarded as processes in which a system with initially N particles evolves in real-time to a system of $N-1$ or $N+1$ particles. The particle number of a system S_1 can only change if it is coupled to a bath S_2. The particle number of the total system-and-bath, i.e. $\mathcal{N} = N_1 + N_2$, is fixed and integer, whereas the particle number N_1 and N_2 can take fractional values. In general, an infinitesimal small kinetic coupling term of a system to a bath lifts the degeneracy of the ground-state of the combined system $S_1 + S_2$ as we have exemplified for the eigenenergies of the two-site model in figure 6, ultimately leading to a smooth density-to-potential map. Functionals of this smooth map are also smooth, as we exemplify in the following sections for the wavefunction and selected observables as functional of the ground-state density. We will see that in the weakly coupled limit, i.e. the limit $\varphi = \frac{\pi}{2} - 1/100$, the straight-line behavior is an excellent approximation to the exact functional behavior along the cut in the variable δn but that the exact functional shows a smooth behavior since the density-to-potential map is also smooth. The deviation of the straight-line behavior depends on the energy-scale of the coupling term between the system and the bath. To see how the functionals deviate from the straight-line behavior we included a zoom of the functionals in the respective limit whenever it improved the clarity. The third case in figure 7(c) is valid for an infinitesimally small coupling of a system to a bath for which the ground-state of the system shows an accidental degeneracy. Here the coupling of

both sites is realized via the long-range soft Coulomb interaction in the Hamiltonian. Functionals of the distributional points of the density-to-potential map are then linear combinations of the densities of the degenerate subspace, and can be connected via straight-lines [25, 70]. For such weakly coupled processes with a degenerate ground-state, the straight-line behavior and hence the derivative discontinuity at integer particle number N introduced in the original work of Perdew is exact.

To give a mathematical more rigorous definition of the concept of the steepening, we introduce the maximum value of the gradient of the effective density-to-potential map, i.e. $f_{ijkl} = \max\left(\frac{\delta n_{ij}}{\delta v_{kl}}\right)$. To obtain the effective density-to-potential map, it is necessary to first partition the density of the system, e.g. using a Bader partitioning scheme. Second, the integrated density over each basin corresponds to a subsystem, e.g. for three subsystems we obtain the densities n_1, n_2 and n_3. To determine the localization and hence, the correlation between two of the three subsystems, we construct the density difference $\delta n_{12} = n_1 - n_2$ and $\delta n_{23} = n_2 - n_3$ as functional of the potential difference, i.e. $\delta n_{12}(\delta v_{12}, \delta v_{23})$ and $\delta n_{23}(\delta v_{12}, \delta v_{23})$, where e.g. $\delta v_{kl} = Z_k - Z_l$ and Z_k is the maximal depth of the external potential present in basin k. The gradient f_{ijkl} is a measure how the localization over subsystems changes subject to small changes in the external effective potential and therefore, can be used to illustrate the intra-system steepening while e.g. stretching the one-dimensional molecule. The size of the tensor f_{ijkl} depends on the number of subsystems present in the system. The steepening presents a slope that gets steeper as the correlation between subsystems in e.g. our bipartite system increases. The relation between δn_{ij} and δv_{kl} remains locally one-to-one and therefore invertible, the domain and co-domain of the selected independent variable and the corresponding functional values can be swapped as long as the corresponding value of f_{ijkl} is bounded. In the limit of the inter-system derivative discontinuity the functional value of f_{ijkl} for given $ijkl$ diverges, indicating that an infinitesimally small change in the effective potential changes the electron localization in the system dramatically. For our specific model system, we illustrate that the transition of the steepening to the non-differentiable derivative discontinuity corresponds to a maximum in the von-Neumann correlation functional which provides a good measure for the correlation present in the system. For systems with degenerate ground-state (each of which corresponds to a Hilbert space with fixed particle number), the ground-state density can be constructed by a linear combination in the degenerate subspace resulting in a straight-line behavior whose slope changes at integer $\delta n = N$. Functionals in these points (at integer N) are not differentiable. Whenever an intra-system steepening in the effective density-to-potential map appears as a consequence of high correlation, we expect such a feature to be present in the xc functional as a functional of the ground-state density.

5. Features of the exact density-to-wavefunction map

The inter-system derivative discontinuity and the intra-system steepening discussed in the previous section are exact properties of the density-to-potential map. As a consequence, also the exact wavefunction and hence, all exact observables as function of the exact density inherit the intra-system steepening and the inter-system derivative discontinuity. In the following sections we illustrate this fact. In particular, we show how these features show up in the CI-coefficients, and consequently in the energy, the excited-densities and in the correlation entropy functional.

5.1. Exact configuration interaction coefficients as functionals of the ground-state density

To construct the density-to-wavefunction map, we expand the correlated ground- and excited-state wavefunctions from the exact diagonalization of the Hamiltonian in a complete set of Slater determinants $|\Phi_q\rangle$. This gives rise to CI coefficients as functionals of the ground-state density as defined in equation (17). Clearly, each choice for the set of Slater determinants $|\Phi_q\rangle$ induces a different set of CI functionals. Here we choose as basis set the determinants which are eigenfunctions of the free kinetic energy operator. More specifically, we project the two-particle singlet ground-state wavefunction of the Hamiltonian in equation (7) onto the three two-particle singlet eigenstates of the kinetic operator $\hat{T}$ to construct one of these sets for each different φ. The results are summarized in figure 8. Each row in the figure displays one of the ground-state CI coefficients as function of the density difference between the sites, $\alpha_q[\delta n_{00}] = \langle\Phi_q|\Psi_0[N = 2, S^2 = 0, S_z = 0, \delta n_{00}]\rangle$. For non-interacting electrons, the CI coefficients can be evaluated analytically. In our chosen basis the coefficients have no explicit dependency on λ_t,

$$\alpha_1^{\varphi=0}[\delta n_{00}] = -\frac{(\delta n_{00}^2 - 2(2 + \sqrt{4 - \delta n_{00}^2}))(2 + |\delta n_{00}|)}{4\sqrt{-(-4 + \delta n_{00}^2)(4 + \delta n_{00}^2 + 4|\delta n_{00}|)}}, \tag{23}$$

$$\alpha_2^{\varphi=0}[\delta n_{00}] = -\frac{\delta n_{00}}{2\sqrt{2}}, \tag{24}$$

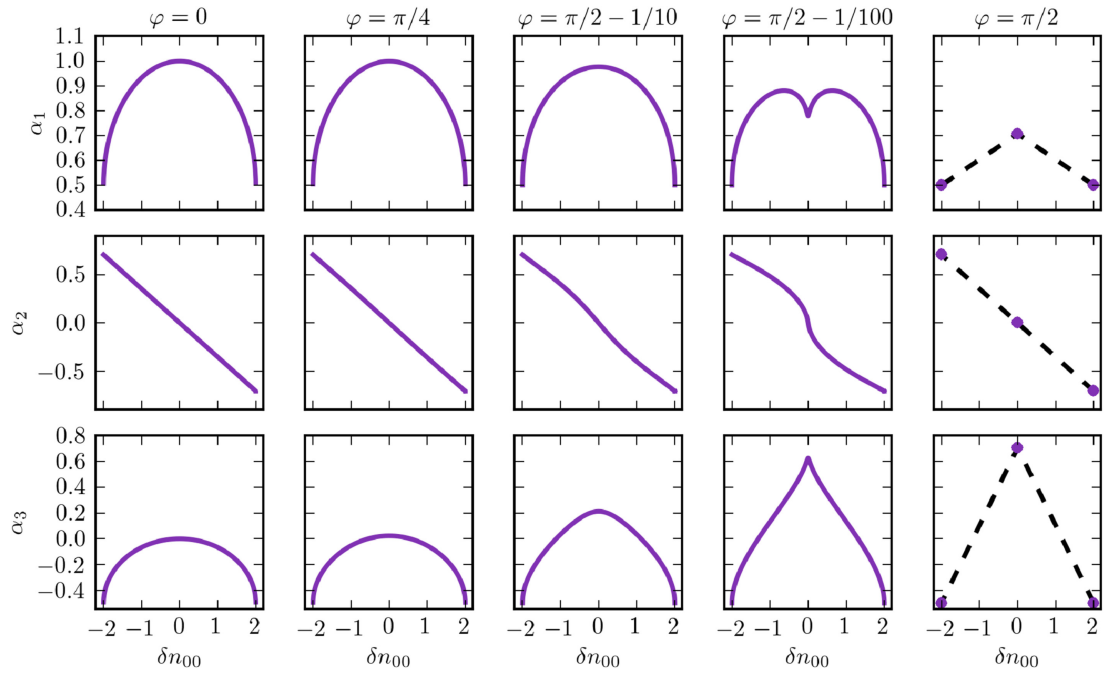

Figure 8. CI coefficients of the two-particle ground-state wavefunction in the kinetic operator basis. From left-to-right we approach the strictly localized limit ($\varphi = \frac{\pi}{2}$) and the gradient of all three CI coefficients steepens. For $\varphi = \frac{\pi}{2}$ the CI coefficients take only discrete values which can be interpolated linearly (dashed lines) due to the degeneracy of the eigenstates in the strictly localized limit.

$$\alpha_3^{\varphi=0}[\delta n_{00}] = -\frac{(-4 + \delta n_{00}^2 + 2\sqrt{4 - \delta n_{00}^2})(2 + |\delta n_{00}|)}{4\sqrt{-(-4 + \delta n_{00}^2)(4 + \delta n_{00}^2 + 4|\delta n_{00}|)}}. \tag{25}$$

The CI coefficients of the non-interacting electrons are shown in the leftmost column of figure 8, where $\varphi = 0$. Approaching the strictly localized electron limit, i.e. from left to right in figure 8, the gradient of the CI coefficients sharpens. This sharpening corresponds to the intra-system steepening of the δn_{00}-to-δv map introduced in section 4 and is inherited by the CI coefficients. Furthermore, the inter-system derivative discontinuity shows up in the CI coefficients for $\varphi = \frac{\pi}{2}$ and the CI functionals become distributional points

$$\alpha_1^{\varphi=\frac{\pi}{2}}[\delta n_{00}] = \begin{cases} \frac{1}{2}, & \text{for } \delta n_{00} = -2 \\ \frac{1}{\sqrt{2}}, & \text{for } \delta n_{00} = 0 \\ \frac{1}{2}, & \text{for } \delta n_{00} = +2, \end{cases}$$

$$\alpha_2^{\varphi=\frac{\pi}{2}}[\delta n_{00}] = \begin{cases} \frac{1}{\sqrt{2}}, & \text{for } \delta n_{00} = -2 \\ 0, & \text{for } \delta n_{00} = 0 \\ -\frac{1}{\sqrt{2}}, & \text{for } \delta n_{00} = +2, \end{cases}$$

$$\alpha_3^{\varphi=\frac{\pi}{2}}[\delta n_{00}] = \begin{cases} -\frac{1}{2}, & \text{for } \delta n_{00} = -2 \\ \frac{1}{\sqrt{2}}, & \text{for } \delta n_{00} = 0 \\ -\frac{1}{2}, & \text{for } \delta n_{00} = +2, \end{cases}$$

which are connected via straight lines due to the degeneracy of the ground-state, see discussion in section 4.1.

5.2. Exact ground-state and excited-state energy functionals

Since the CI coefficients α_q^φ of the wavefunction inherit the intra-system steepening and the inter-system derivative discontinuity, arbitrary ground-state expectation values, defined in equation (18), also inherit the intra-system steepening and the inter-system derivative discontinuity. Note, the excited-state CI coefficients also show the same exact features, which are then inherited by excited-state functionals in the respective limit. As particular examples for this inheritance, we illustrate in figure 9 the intra-system steepening and the inter-system derivative discontinuity for the exact Hohenberg–Kohn functional ($j = 0$) and the excited-state energy

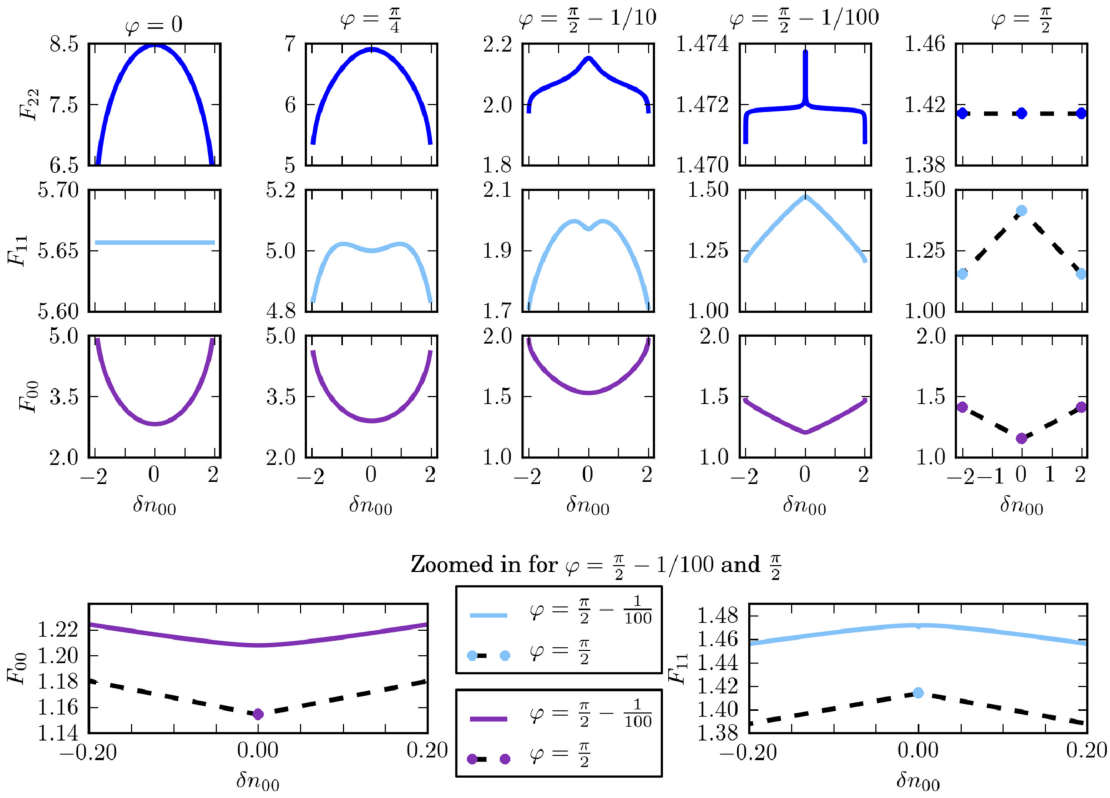

Figure 9. Exact energy functionals $F_{jj} = \langle\Psi_j|\ \lambda_t(\varphi)\hat{T} + \lambda_w(\varphi)\hat{W}\ |\Psi_j\rangle$ of the ground-, the first- and second-excited state for different strengths of the electron localization φ. First row: second excited-state energy F_{22} as functional of the ground-state density. Second row: first excited-state energy F_{11} as functional of the ground-state density. Third row: ground-state energy F_{00} as functional of the ground-state density, i.e. the Hohenberg–Kohn functional. From the non-interacting limit (left) to the strictly localized limit (right), the gradient of all energy functionals steepens. In the highly localized limit, where $\varphi = \frac{\pi}{2} - \frac{1}{100}$, all energy functionals are continuous. In particular, the ground-state energy functional shows a convex behavior as can be seen in the detailed view of the intra-system steepening of highly localized electrons and the inter-system derivative discontinuity of strictly localized electrons at the bottom of the figure. Note, that here the x-axis has been scaled by one order of magnitude. In the strictly localized limit, for all energy functionals only the three distributional points $\delta n_{00} = \pm 2$ and $\delta n_{00} = 0$ exist. Due to the degeneracy of the eigenstates in the strictly localized limit which is shown in the lower panel of figure 6, these three distributional points connect via straight lines indicated by a black-dashed line.

functionals ($j = 1, 2$)

$$F^{\varphi}_{jj}[\delta n_{00}] = \langle\Psi^{\varphi}_{2s,j}|\ \lambda_t(\varphi)\hat{T} + \lambda_w(\varphi)\hat{W}\ |\Psi^{\varphi}_{2s,j}\rangle, \tag{26}$$

for the two-particle singlet states $|\Psi^{\varphi}_{2s,j}\rangle = |\Psi^{\varphi}_{j}[\delta n_{00},\ N = 2,\ S^2 = 0,\ S_z = 0]\rangle$. The third row of figure 9 shows the exact Hohenberg–Kohn functional ($j = 0$) discussed previously in literature [43–46], the first and second row show the first and second excited-state energy functional ($j = 1, 2$), respectively. The gradient of all three functionals $F_{jj}[\delta n_{00}]$ steepens approaching the limit of strictly localized electrons, just as previously observed for the density-to-potential map in section 4 and the density-to-wavefunction map in section 5.1. However, if φ differs infinitesimally from the strictly localized limit, all energy functionals are continuous. In particular, the ground-state energy functional F_{00} is convex. The difference between the highly localized and the strictly localized limit, is displayed in an inset at the bottom in figure 9, which contains a zoom of the critical region of the ground- and first excited-state state functional. Here, in the limit of strictly localized electrons, in which both sites are kinetically decoupled, the intra-system steepening transitions into the inter-system derivative discontinuity. As already discussed for the density-to-wavefunction map, the distributional points can be connected via straight lines due to the degeneracy of the eigenstates in this limit.

5.3. Exact excited- and transition density functionals

To illustrate the fact that all physical observables inherit the intra-system steepening and the inter-system derivative discontinuity, we also show the excited- ($k = j = 1, 2$) and transition-state densities ($k \neq j = 0, 1, 2$)

$$\delta n_{kj}[\delta n_{00}] = \langle\Psi_k[\delta n_{00}, N]|\ \hat{O}\ |\Psi_j[\delta n_{00}, N]\rangle \tag{27}$$

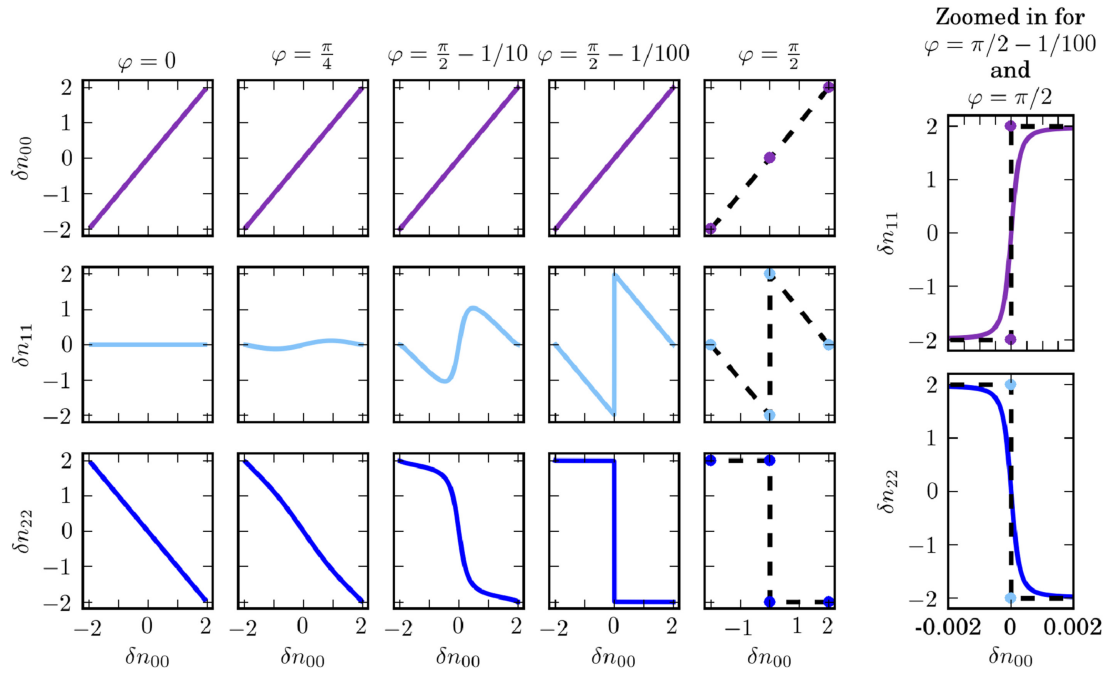

Figure 10. Density functionals for ground- and excited-singlet states. First panel: ground-state density as functional of the ground-state density. Second panel: first excited-state density as functional of the ground-state density. Third panel: second excited-state density as functional of the ground-state density. From the non-interacting limit (left) to the strictly localized limit (right), the gradient of all excited-state density functionals steepens. A detailed view of the intra-system steepening for highly localized electrons $\left(\varphi = \frac{\pi}{2} - \frac{1}{100}\right)$ and the inter-system derivative discontinuity is given on the right.

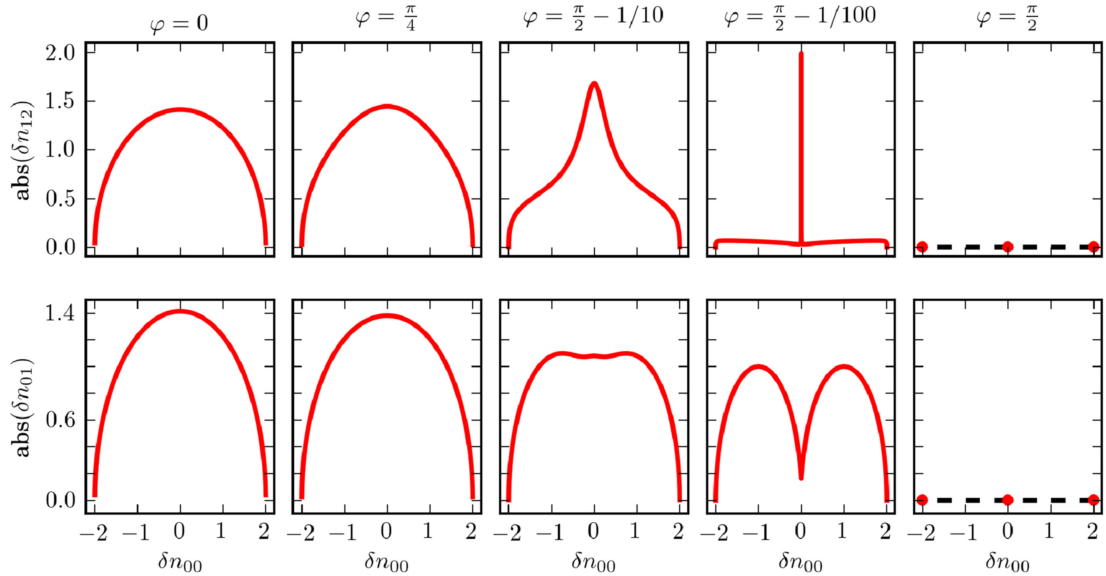

Figure 11. Transition matrix elements of the density operator between different excited many-body states as functional of the ground-state density $\delta n_{jk} = \langle \Psi_j | \ \delta\hat{n} \ | \Psi_k \rangle$. First row: absolute value of the exact transition density from the first and second excited-state as functional of the ground-state density $\delta n_{12}(\delta n_{00})$. Second row: absolute value of the exact transition density from the ground-and the first excited-state as functional of the ground-state density $\delta n_{01}(\delta n_{00})$. From the non-interacting (left) to the strictly localized limit (right), approaching the strictly localized limit the gradient of both transition density functionals steepens. In the strictly localized limit, the sites are disconnected. Therefore, there are no transitions between the three two-particle singlet states, and the transition densities are zero.

as functionals of the ground-state density δn_{00}. The excited-state density functionals are shown in the second and third row of figure 10 respectively. For completeness, also the trivial linear behavior of the ground-state density as functional of the ground-state density is shown in the first row of the figure. From the non-interacting (left) to the strictly localized limit (right), the gradient of the excited-state density functionals steepens up to the

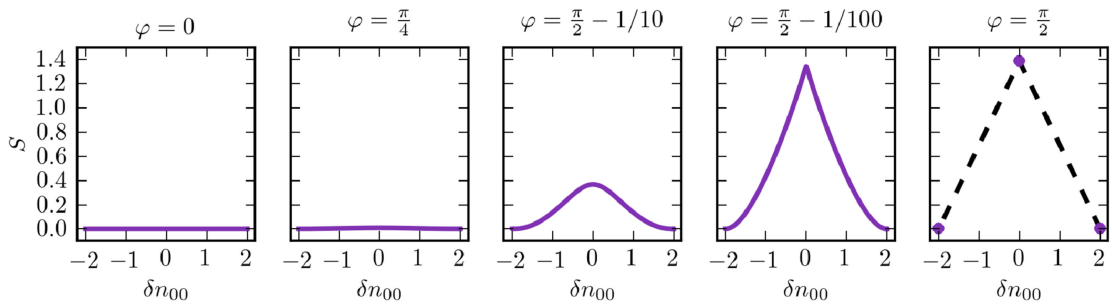

Figure 12. Correlation entropy as functional of the ground-state density indicating the correlation within the system. For non-interacting electrons the correlation entropy is zero. From left to right, approaching the strictly localized limit, the correlation and the mixing of the eigenstates and hence the correlation entropy increases. Furthermore, the gradient of the functional obeys the intra-system steepening and the inter-system derivative discontinuity for $\varphi = \frac{\pi}{2}$.

strictly localized limit where the excited-state density functionals obey the straight-line condition due to the degeneracy of the ground-state. To highlight the difference of the intra-system steepening and inter-system derivative discontinuity of the excited-state density functionals a detailed view of the critical region can be found on the right-hand side of figure 10.

Transition densities are an important ingredient for linear response calculations in time-dependent DFT. For our model system, we show the exact transition densities as functionals of the ground-state density. In contrast to the excited-state density functionals, the transition density functionals are phase-dependent. Figure 11 shows the absolute value of the transition density as functional of the ground-state density. The first and second row of figure 11 show the absolute value of the transition density from the first to the second and from the ground- to the second excited state, respectively. Approaching the strictly localized limit, both transition-state densities show clearly the intra-system steepening. In the strictly localized limit, there is no transition between the eigenstates of the system and the transition-state densities are zero, see $\varphi = \frac{\pi}{2}$ in panel one and two.

5.4. Exact correlation entropy functional

As final example we illustrate the functional behavior of the correlation entropy. The correlation entropy , discussed in detail in [38] measures the correlation and entanglement present in a many-body system. It can be understood as well as a measure of the Slater rank [38, 39] as can be seen if we compare the correlation entropy plotted in figure 12 with the mixing of the eigenstates in lower panel and inset of figure 6 for the different values of the parameter φ. In the two-site model, where we have access to all eigenvectors and eigenvalues, we can compute the correlation entropy of the system

$$S = \sum_{j=1}^{\infty} n_j \ln n_j, \tag{28}$$

where n_j are the eigenvalues of the reduced one-body density matrix

$$\rho_{00}(j\sigma, j'\sigma') = \langle \Psi_0 |\ \hat{c}^{\dagger}_{j\sigma} \hat{c}_{j'\sigma'}\ | \Psi_0 \rangle. \tag{29}$$

The correlation entropy is zero for pure states, and has its maximum for maximally mixed states [38, 39, 71]. In figure 12 we see that the correlation entropy increases with increasing correlation while the gradient of the correlation entropy functional obeys the intra-system steepening and transitions into the inter-system derivative discontinuity due to the degeneracy of the ground-state for $\varphi = \frac{\pi}{2}$. In the limit of non-interacting electrons, where there is no correlation, the correlation entropy vanishes. The maximum value of the correlation entropy is reached in the strictly localized limit for $\delta n_{00} = 0$ where all three eigenenergies are degenerate.

6. Summary

In the present work we have illustrated for a simple but general interacting lattice model how the intra-system steepening, an exact feature of the ground-state density-to-potential map, develops gradually with increasing decoupling between fragments of a system and transforms into the well-known inter-system derivative discontinuity for an accidental degeneracy of the ground-state of weakly coupled systems. As a consequence of the Hohenberg–Kohn theorem, the wavefunction-to-density map inherits the exact features of the density-to-potential map as well as the ground- and excited-state observables and transition-matrix elements.

Although both exact features are linked to the localization of the electrons, we carved out that the intra-system steepening and the inter-system derivative discontinuity are conceptually different features within density functional theory. The inter-system derivative discontinuity corresponds to the electron localization in weakly coupled subsystems with degenerate ground-state. The inter-system derivative discontinuity coincides with a real crossing of the eigenenergies of the system as function of the external potential. In this limit, the cut along the variable δn of the generally very high-dimensional ground-state density functionals have straight lines between different values for the particle number N due to the mixture of the states in degenerate subspaces, $F = (1 - \omega)F_N + \omega F_{N+1}$ with the mixing parameter $0 \leqslant \omega \leqslant 1$. The intra-system steepening instead corresponds to the electron localization in weakly to strong coupled fragments of a system. The intra-system steepening coincides with an avoided crossing of the eigenenergies as function of the external potential and sharpens when approaching the real crossing. Ground-state density functionals result directly from the one-to-one correspondence of the Hohenberg–Kohn theorem, such as the convex ground-state energy as function of the density difference between the fragments of the system.

The inter-system derivative discontinuity plays a crucial role whenever the particle number of the total system changes which is the case for observables such as the electron affinity $A = E[N] - E[N + 1]$, the ionization energy $I = E[N - 1] - E[N]$, the fundamental gap which is the difference of ionization energy and affinity $E_{\text{gap}} = I - A$, and the chemical hardness $\eta = \left(\frac{\partial^2 E}{\partial N^2}\right)_v$ of a system. The intra-system steepening is linked to processes where particles are transferred from one fragment to another within a system of fixed particle number such as stretched molecules, charge-transfer processes and any problem involving highly localized electrons. We expect approximate functionals may fail to describe such problems because of the lack of the intra-system steepening feature. Given the relevance of the above mentioned problems it is crucial to develop improved density functionals that capture this exact condition of the exact density-to-potential and density-to-wavefunction maps. In the highly localized electron limit the exact xc-functional does not present a straight line behavior but rather a sharp but differentiable one.

Our work illustrates those fundamental concepts of density functional theory. To improve the accuracy of DFT observables, approximate functionals should capture both, the inter-system derivative discontinuity and the intra-system steepening respectively. Work about how to generalize the present results from lattice Hamiltonians to real-space systems is currently in progress. Our results also allow to get insight about spin DFT functionals as the magnetization of the N electron system can be written in terms of the ground-state density (as all other observables we discussed in this paper). This is a way to solve the known problems of spin DFT [72, 73] (however it would require going beyond present adiabatic functionals, work along those lines is in progress).

Acknowledgments

The authors thank Professor Matthias Scheffler for his support, Johannes Flick, Jessica Walkenhorst and Viktor Atalla for very useful discussions and comments, and Nicola Kleppmann, Teresa Reinhard and Anne Hodgson for comments on the manuscript. We acknowledge financial support from the European Research Council Advanced Grant DYNamo (ERC-2010- AdG-267374), Spanish Grant (FIS2013-46159-C3-1-P), Grupos Consolidados UPV/EHU del Gobierno Vasco (IT578-13), COST Actions CM1204 (XLIC), and MP1306 (EUSpec).

References

[1] Baerends E J and Gritsenko O V 1997 *J. Phys. Chem.* A **101** 5383
[2] Capelle K 2006 *Braz. J. Phys.* **36** 1318
[3] Ziegler T 1991 *Chem. Rev.* **91** 651
[4] Kohn W, Becke A D and Parr R G 1996 *J. Phys. Chem.* **100** 12974
[5] Pribram-Jones A, Gross D A and Burke K 2015 *Annu. Rev. Phys. Chem.* **66** 283
[6] Kohn W and Sham L J 1965 *Phys. Rev.* **140** A1133
[7] Perdew J P, Burke K and Ernzerhof M 1996 *Phys. Rev. Lett.* **77** 3865
[8] Becke A D 1993 *J. Chem. Phys.* **98** 5648–52
[9] Kümmel S and Kronik L 2008 *Rev. Mod. Phys.* **80** 3
[10] Heyd J, Scuseria G E and Ernzerhof M 2003 *J. Chem. Phys.* **118** 8207
[11] Xiao H, Tahir-Kheli J and Goddard W A 2011 *J. Phys. Chem. Lett.* **2** 212
[12] Caruso F, Rohr D R, Hellgren M, Ren X, Rinke P, Rubio A and Scheffler M 2013 *Phys. Rev. Lett.* **110** 146403
[13] Cohen A J, Mori-Sánchez P and Yang W 2012 *Chem. Rev.* **112** 289
[14] Champagne B, Perpte E A, van Gisbergen S J A, Baerends E-J, Snijders J G, Soubra-Ghaoui C, Robins K A and Kirtman B 1998 *J. Chem. Phys.* **109** 10489
[15] van Gisbergen S J A, Schipper P R T, Gritsenko O V, Baerends E J, Snijders J G, Champagne B and Kirtman B 1999 *Phys. Rev. Lett.* **83** 694
[16] Jacob C R and Reiher M 2012 *Int. J. Quantum Chem.* **112** 3661

[17] Kronik L, Stein T, Refaely-Abramson S and Baer R 2012 *J. Chem. Theory Comput.* **8** 1515
[18] Kraisler E and Kronik L 2015 *Phys. Rev.* A **91** 032504
[19] Kraisler E and Kronik L 2013 *Phys. Rev. Lett.* **110** 126403
[20] Li C, Zheng X, Cohen A J, Mori-Sánchez P and Yang W 2015 *Phys. Rev. Lett.* **114** 053001
[21] Armiento R and Kümmel S 2013 *Phys. Rev. Lett.* **111** 036402
[22] van Aggelen H, Yang Y and Yang W 2013 *Phys. Rev.* A **88** 030501
[23] Cohen A J, Mori-Sánchez P and Yang W 2008 *Science* **321** 792
[24] Mori-Sánchez P, Cohen A J and Yang W 2008 *Phys. Rev. Lett.* **100** 146401
[25] Perdew J P, Parr R G, Levy M and Balduz J L 1982 *Phys. Rev. Lett.* **49** 1691
[26] Vydrov O A and Scuseria G E 2006 *J. Chem. Phys.* **125** 234109
[27] Seidl M 1999 *Phys. Rev.* A **60** 4387
[28] Seidl M, Gori-Giorgi P and Savin A 2007 *Phys. Rev.* A **75** 042511
[29] Gori-Giorgi P, Seidl M and Vignale G 2009 *Phys. Rev. Lett.* **103** 166402
[30] Mirtschink A, Seidl M and Gori-Giorgi P 2013 *Phys. Rev. Lett.* **111** 126402
[31] Buijse M A, Baerends E J and Snijders J G 1989 *Phys. Rev.* A **40** 4190
[32] van Leeuwen R and Baerends E J 1994 *Phys. Rev.* A **49** 2421
[33] Gritsenko O, van Leeuwen R and Baerends E J 1994 *J. Chem. Phys.* **101** 8955
[34] Gritsenko O V, van Leeuwen R and Baerends E J 1995 *Phys. Rev.* A **52** 1870
[35] Gritsenko O V and Baerends E J 1996 *Phys. Rev.* A **54** 1957
[36] Tempel D G, Martínez T J and Maitra N T 2009 *J. Chem. Theory Comput.* **5** 770
[37] Helbig N, Tokatly I V and Rubio A 2009 *J. Chem. Phys.* **131** 224105
[38] Ziesche P, Gunnarsson O, John W and Beck H 1997 *Phys. Rev.* B **55** 10270
[39] Schliemann J, Cirac J I, Kuś M, Lewenstein M and Loss D 2001 *Phys. Rev.* A **64** 022303
[40] Cuevas-Saavedra R, Ayers P W and Staroverov V N 2015 *J. Chem. Phys.* **143** 244116
[41] Ryabinkin I G, Kohut S V and Staroverov V N 2015 *Phys. Rev. Lett.* **115** 083001
[42] Cuevas-Saavedra R and Staroverov V N 2016 *Mol. Phys.* **114** 1050–8
[43] Capelle K, Lima N, Silva M and Oliveira L 2003 *The Fundamentals of Electron Density, Density Matrix and Density Functional Theory in Atoms, Molecules and the Solid State* (*Progress in Theoretical Chemistry and Physics* vol 14) ed N Gidopoulos and S Wilson (Netherlands: Springer) pp 145–68
[44] Carrascal D J and Ferrer J 2012 *Phys. Rev.* B **85** 045110
[45] Carrascal D J, Ferrer J, Smith J C and Burke K 2015 *J. Phys.: Condens. Matter* **27** 393001
[46] Fuks J I, Farzanehpour M, Tokatly I V, Appel H, Kurth S and Rubio A 2013 *Phys. Rev.* A **88** 062512
[47] Hohenberg P and Kohn W 1964 *Phys. Rev.* **136** B864
[48] Gunnarsson O and Schönhammer K 1986 *Phys. Rev. Lett.* **56** 1968
[49] Schönhammer K, Gunnarsson O and Noack R M 1995 *Phys. Rev.* B **52** 2504
[50] Fuks J I and Maitra N T 2014 *Phys. Chem. Chem. Phys* **16** 14504
[51] Fuks J I and Maitra N T 2014 *Phys. Rev.* A **89** 062502
[52] Fuks J I, Elliott P, Rubio A and Maitra N T 2013 *J. Phys. Chem. Lett.* **4** 735
[53] Wagner L O, Stoudenmire E M, Burke K and White S R 2012 *Phys. Chem. Chem. Phys.* **14** 8581
[54] Thiele M, Gross E K U and Kümmel S 2008 *Phys. Rev. Lett.* **100** 153004
[55] Thiele M and Kümmel S 2009 *Phys. Chem. Chem. Phys.* **11** 4631
[56] Wagner L O, Stoudenmire E M, Burke K and White S R 2013 *Phys. Rev. Lett.* **111** 093003
[57] Wagner L O, Baker T E, Stoudenmire E M, Burke K and White S R 2014 *Phys. Rev.* B **90** 045109
[58] Baer R 2010 *Phys. Rev. Lett.* **104** 073001
[59] Kryachko E S and Ludea E V 1991 *Phys. Rev.* A **43** 2179
[60] Kohn W 1983 *Phys. Rev. Lett.* **51** 1596
[61] Englisch H and Englisch R 1983 *J. Phys. A: Math. Gen.* **16** L693
[62] Englisch H and Englisch R 1983 *Physica* A **121** 253
[63] Chayes J, Chayes L and Ruskai M 1985 *J. Stat. Phys.* **38** 497
[64] Levy M 1982 *Phys. Rev.* A **26** 1200
[65] Lieb E H 1983 *Int. J. Quantum Chem.* **24** 243
[66] Mori-Sánchez P and Cohen A J 2014 *Phys. Chem. Chem. Phys.* **16** 14378
[67] Cohen A J and Mori-Sánchez P 2014 *J. Chem. Phys.* **140** 044110
[68] Bader R F W, Beddall P M and Cade P E 1971 *J. Am. Chem. Soc.* **93** 3095
[69] Henkelman G, Arnaldsson A and Jónsson H 2006 *Comput. Mater. Sci.* **36** 354
[70] Yang W, Zhang Y and Ayers P W 2000 *Phys. Rev. Lett.* **84** 5172
[71] Franco I and Appel H 2013 *J. Chem. Phys.* **139** 094109
[72] Eschrig H and Pickett W 2001 *Solid State Commun.* **118** 123
[73] Capelle K and Vignale G 2001 *Phys. Rev. Lett.* **86** 5546